

Magnetic structure of selected Gd intermetallic alloys from first principles

L. Petit^{1,*}, Z. Szotek¹, D. Paudyal², A. Biswas², Y. Mudryk², V. K. Pecharsky^{2,3} and J. B. Staunton⁴

¹Daresbury Laboratory, Daresbury, Warrington WA4 4AD, United Kingdom

²The Ames Laboratory, US Department of Energy, Iowa State University, Ames, Iowa 50011-3020, USA

³Department of Materials Science and Engineering, Iowa State University, Ames, Iowa 50011-2300, USA

⁴Department of Physics, University of Warwick, Coventry CV4 7AL, United Kingdom



(Received 6 August 2019; revised manuscript received 1 November 2019; published 8 January 2020)

Using first-principles calculations, based on disordered local moment (DLM) theory combined with the self-interaction corrected local spin density approximation (SIC-LSDA), we study magnetic correlations in the paramagnetic state of GdX ($X = \text{Cu, Zn, Ga, Ag, Cd, In, Au, Hg, and Tl}$) intermetallics and their alloys. The predicted magnetic orders and ordering temperatures that these correlations lead to are in overall good agreement with available experiments. The interactions between the Gd f -electron local moments are mediated by the valence electrons of the intermetallics which comprise both Gd and X d bands as well as sp bands. There are RKKY-like features such as dependence on the number of sp -valence electrons but other variations manifest themselves in the phase diagrams as regions of incommensurate magnetic ordering, the origin and range of which are related to the binding energies of the alloying anion d states, and their propensity to hybridize with the Gd states at the Fermi level.

DOI: [10.1103/PhysRevB.101.014409](https://doi.org/10.1103/PhysRevB.101.014409)

I. INTRODUCTION

The rare-earth (R) intermetallic compounds, in particular those formed with the elements of the IB, IIB, and IIIA groups of the Periodic Table, and crystallizing in the simple CsCl structure, have been extensively investigated experimentally for many years [1–7]. Owing to their structural simplicity and a variety of observed magnetic properties, they have been of interest for understanding the magnetic properties and mechanisms driving the magnetic interactions between the $4f$ moments observed in these materials. In particular, establishing whether a simple Ruderman-Kittel-Kasuya-Yosida (RKKY) model [8] can adequately describe the exchange interaction between the f -electron moments and/or what is behind any deviations from it, has long been the interest of many studies. As some experiments showed considerable deviations from the RKKY model, Campbell [9] pointed out that the $5d$ electrons of the rare earths could play an essential role in the indirect exchange interaction and thus should be given a thorough consideration in all theoretical studies. Consequently, also the overlap of the $5d$ electrons with the d electrons of the anions (X) forming the intermetallic compounds, as well as their solid solutions with the rare earths, should be properly accounted for with respect to their influence on those exchange interactions.

Regarding the magnetic ordering, many experiments looked into the importance of the number of conduction electrons and the site separations, as well as the concentration of different species in the rare-earth intermetallic alloys. Among the frequently studied intermetallic alloys are $\text{RZn}_x\text{Cu}_{1-x}$, $\text{RIn}_x\text{Ag}_{1-x}$, $\text{GdZn}_x\text{Ag}_{1-x}$, and $\text{GdIn}_x\text{Zn}_{1-x}$ [4,5,7,10–13]. It has been observed that the intermetallic compounds formed

with the heavy lanthanide elements and the group IB elements, Cu, Ag, and Au, are usually antiferromagnetic [4], while those formed with the group IIB elements, Zn, Cd, and Hg, are ferromagnetic. In the intermetallic compounds formed with In and Tl, representing the IIIA group, the magnetic order is again antiferromagnetic (GdGa crystallizing in the CrB structure is found to be ferromagnetic [14]). This change from anti- to ferro- and back to antiferromagnetism, associated with the change of sign of the magnetic interaction, indicates that the number of conduction electrons plays a decisive role in determining the magnetic structures [15].

With respect to the theoretical description of rare-earth intermetallics magnetism, model calculations relying on phenomenological parameters have been very successful in describing the possible mechanisms behind the magnetic ordering, but fully first-principles quantitative calculations remain a challenge owing to the strongly localized nature of the lanthanide $4f$ electrons. The development of first-principles methodologies based on density functional theory (DFT), in either its local spin density approximation (LSDA) or generalized gradient approximation (GGA) to exchange and correlation, has resulted in considerable advances in the understanding of transition metal based magnetism, both with respect to ground-state properties and finite temperature fluctuations [16]. However, the localized nature of $4f$ electrons cannot be straightforwardly described within a simple band picture approach. The LSDA, and even GGA, due to an unphysical self-interaction problem [17], cannot adequately account for the electron-electron interactions that tend to localize the f electrons on sites and, in order to address this shortcoming, it is required to include an additional *ab initio* correction [18,19], or parameters that are most commonly derived from experiment [20], but can also be calculated [21–23].

*leon.petit@stfc.ac.uk

In the present paper, combining the self-interaction corrected (SIC)-LSDA approach [19] with the disordered local moment (DLM) theory [16], and coherent potential approximation (CPA) to deal with chemical disorder [24], we overcome these hurdles and, by studying magnetic correlations in the paramagnetic state, predict the magnetic orders and transition temperatures for a range of binary GdX ($X=\text{Cu, Zn, Ga, Ag, Cd, In, Au, Hg, and Tl}$) compounds and their alloys. Some of the ordered compounds have been reported in our earlier works, both at ambient conditions and under pressure [25,26], but are also included here for completeness and the sake of discussing trends.

The paper is organized as follows. In Sec. II, we briefly describe our method. Section III presents results for the ordered GdX intermetallics, while Sec. IV shows the results we have calculated for alloys of some Gd intermetallics and their comparison with available experimental data. A detailed discussion and analysis of the results both for the ordered compounds and alloys is presented in Sec. V. The paper is concluded in Sec. VI. Technical details of the calculations are given in Appendix A, while in Appendix B, we discuss our experimental measurements and results for a few small concentrations of Ga in the $\text{GdGa}_x\text{Zn}_{1-x}$ alloys.

II. THEORY

In the combined theoretical approach we use, the disordered local moment theory handles the magnetic fluctuations, whilst the self-interaction correction removes from LSDA an unphysical interaction of an electron with itself to provide an adequate description of f electron correlations and localization [27]. In DLM theory, local moments of fixed magnitudes are assumed to persist to high temperatures and in Gd intermetallics they are formed naturally from partially occupied localized $4f$ -electron states. The orientations of these moments fluctuate slowly compared to the dynamics of the valence electron glue surrounding them. By labeling these transverse modes by local spin polarization axes $\hat{\mathbf{e}}_i$, fixed to each lanthanide atom i , and using a generalization of spin density functional theory (SDFT) [16] (+SIC [28,29]) for prescribed orientational arrangements, $\{\hat{\mathbf{e}}_i\}$, we can determine the ab-initio energy for each configuration, $\Omega\{\hat{\mathbf{e}}_i\}$, so that the configuration probability at a temperature T can be found. The magnetic state of the system is set by local averages, or order parameters, $\{\mathbf{m}_i = \langle \hat{\mathbf{e}}_i \rangle\}$, where the magnitudes $m_i = |\mathbf{m}_i|$ range from 0 for the fully disordered high temperature paramagnetic (PM) state to 1 when the magnetic order is complete at $T = 0\text{K}$.

The thermal average of the energy, $\langle \Omega\{\hat{\mathbf{e}}_i\} \rangle = \bar{\Omega}(\{\mathbf{m}_i\})$, depends on the magnetic order parameters, $\{\mathbf{m}_i\}$. The electronic charge density and also the magnetization density, which sets the moment magnitudes $\{\mu_i\}$ [16], are determined self-consistently in the DFT sense. The full Gibbs free energy of a system, magnetic phase diagrams and associated caloric effects can be found using recent developments to DLM theory [25,30,31]. In this paper, we focus on the pair correlations between the local moments in the high temperature paramagnetic state in order to identify the likely magnetically ordered states to form at lower temperatures. To this end, using linear response theory, we calculate the paramagnetic

spin susceptibility,

$$\chi(\mathbf{q}, T) = \frac{\mu^2}{3k_B T - S^{(2)}(\mathbf{q}, T)}, \quad (1)$$

where $S^{(2)}(\mathbf{q}, T)$ is the lattice Fourier transform (LFT) of the direct correlation function [16,29],

$$S_{ij}^{(2)}(T) = \frac{\delta^2 \bar{\Omega}(\{\mathbf{m}_i\}, T)}{\delta \mathbf{m}_i \delta \mathbf{m}_j} \Big|_{\{\mathbf{m}_i=0\}}, \quad (2)$$

and the transition temperature for a second order transition can be directly obtained from $T_c = S^{(2)}(\mathbf{q}_{\max}, T_c)/3k_B$, where \mathbf{q}_{\max} is the wave vector for which $S^{(2)}(\mathbf{q}, T)$ is maximal, and it characterizes the nature of the magnetic order below T_c . For example, $\mathbf{q}_{\max} = \mathbf{0}$ describes ferromagnetic order, whereas $\mathbf{q}_{\max} = [00\frac{1}{2}]$ in the Brillouin zone of the cubic CsCl lattice describes an antiferromagnetic state. For the Gd intermetallics, the $S_{ij}^{(2)}$'s play the role of interactions between the Gd $4f$ -electron local moments and contain the response of the materials valence electrons to the magnetic fields that the local moments set up. In essence they capture the physics that the famous RKKY interactions address but include the complexity from a richer valence electronic structure comprising d as well as sp states [25,29,31].

The present DLM + SIC methodology [28,29] has been implemented in the self-consistent field (SCF)-Korringa-Kohn-Rostoker (KKR) multiple scattering theory [32], utilizing the muffin-tin (MT) approximation and including also the coherent potential approximation (CPA) [24,33], the best mean-field treatment of disorder available. Here, the CPA ‘‘machinery’’ has been used for both the ensemble averaging of the constituents alloying (chemical disorder), as well as, averaging over the different local moment orientational configurations dealt with in DLM theory.

In a random substitutional alloy, $A_x B_{1-x}$, where x is the concentration of the A species, like in an ordered compound, the crystal lattice has full periodicity, but the lattice sites are randomly populated by either A or B species. In the CPA approximation, one defines an effective medium, where the potential on a given site is replaced by an effective, coherent, potential, determined from a self-consistency condition stating that if such an effective potential on a lattice site gets replaced by either A or B potential, on average there should be no further scattering from the lattice. This approximation is based on the assumption that the lattice sites are uncorrelated, meaning that any short-range- or long-range-concentration correlations which may exist are neglected. To treat the former, one could use the multiconfiguration or molecular CPA [34], while the latter could be described within the multiatom per cell CPA [35–37], but neither is considered in the present study. Here, we use the standard CPA for an adequate treatment of the chemical disorder of the Gd intermetallic alloys, while the DLM theory describes how valence electrons mediate the interactions between the f electron moments [29]. These can turn out to be RKKY-like, but can also show strong deviations from this picture as we find here.

It should be stressed that the spin fluctuations that are described in this paper are the orientational degrees of freedom of the f -electron local moments on the Gd atoms which vary on a timescale long compared to the other electronic degrees

TABLE I. A comparison of the experimental and calculated data for a number of GdX compounds. Column 1: compound and column 2: experimental crystal structures, columns 3–6 and 7–10: respectively experimental and calculated values for lattice constant (Å), magnetic order, transition temperature (K), pressure derivative of transition temperature (K kbar⁻¹). The experimental lattice parameters in column 3 are derived from the observed experimental volumes as $V^{1/3}$. AF in column 4 indicates antiferromagnetic ordering where the propagation vector has not been determined experimentally. The transition temperature T_c refers to the Néel temperature T_N or Curie temperature T_C depending on order.

GdX	Experiment					Theory			
	Struc.	a	Order	T_c	$\frac{dT_c}{dP}$	a	Order	T_c	$\frac{dT_c}{dP}$
GdCu	CsCl/FeB [39,40]	3.50 [39]	AF-B [40]	150 [40]	0.27 [41], 0.03 [42]	3.43	AF-B	45	0.02
GdAg	CsCl [39]	3.65 [39]	AF-B [43]	132–155 [44–46]	0.43 [42], 1.10 [41]	3.60	AF-B	57	0.08
GdAu	CsCl/CrB [2,47]	3.59 [2]	AF	37 [48]	–	3.58	AF-B	44	0.12
GdZn	CsCl [2]	3.60 [2]	F	270 [2]	–0.13	3.52	F	210	–0.52
GdCd	CsCl [2]	3.75 [2]	F	265 [49]	1.60	3.70	F	231	1.50
GdHg	CsCl [2]	3.72 [2]	–	–	–	3.70	F	133	1.60
GdGa	CrB [50]	3.65 [50]	F	200 [14]	–	3.54	AF-A	42	–
GdIn	CsCl [39]/Tet [46]	3.83 [39], 3.77 [46]	AF	28 [45], 175 [46]	–	3.72	AF-A	51	–
GdTl	CsCl [2,39]/Tet [46,51]	3.78 [39]	AF	<200 [52]	–	3.76	AF-A	98	–

of freedom. These local moments each have a magnitude $\sim 7 \mu_B$ which is rather insensitive to local environments. Any longitudinal spin fluctuations are assumed to be on a much faster time scale and are incorporated into the usual DFT exchange and correlation energy. The DLM picture is therefore very well-suited for the studied here GdX compounds.

III. ORDERED COMPOUNDS

In this section, we focus on a number of Gd intermetallics. As we are mostly interested in studying trends, in the calculations we assume that all of them crystallize in the CsCl structure although, as can be seen in Table I, for some of the compounds conflicting structural data exist.

In the CsCl structure, the Gd ions form a simple cubic lattice, with the anion placed at the center of the cube, forming itself a simple cubic lattice with the origin displaced by $[\frac{1}{2} \frac{1}{2} \frac{1}{2}]$. The Brillouin zone of the primitive cubic CsCl lattice is characterized by three symmetry points corresponding to the wave vectors $\mathbf{k} = [00\frac{1}{2}]$, $\mathbf{k} = [0\frac{1}{2}\frac{1}{2}]$, and $\mathbf{k} = [\frac{1}{2}\frac{1}{2}\frac{1}{2}]$ [38]. In the following, if a compound orders antiferromagnetically with the characteristic wave vector $\mathbf{k} = [00\frac{1}{2}]$, we shall refer to this order as AF-A type, while if the antiferromagnetic order is characterized by the wave vector $\mathbf{k} = [0\frac{1}{2}\frac{1}{2}]$, then we shall refer to it as an AF-B type. AF-C type refers to the antiferromagnetic order corresponding to the wave vector $\mathbf{k} = [\frac{1}{2}\frac{1}{2}\frac{1}{2}]$ (see Fig. 1), but is of no relevance in the present study. The ferromagnetic order is characterized by $\mathbf{k} = [000]$.

As observed in our earlier SIC-LSDA calculations [29], Gd is in the trivalent ground-state configuration, Gd³⁺, with seven localized 4*f* electrons constituting a half-filled shell. Thanks to the latter, spin-orbit coupling, quadrupolar, and crystal field effects, can be safely ignored to first approximation. Consequently, in all our calculations for GdCu, GdZn, GdGa, GdAg, GdCd, GdIn, GdAu, GdHg, and GdTl, the Gd ion is assumed to occur in the Gd(4*f*⁷) configuration, and the corresponding results, in comparison with experiments, are summarized in Table I. Before discussing the latter in detail, it is useful to mention here that the MT approximation utilized

in the SCF-KKR-CPA approach results in the calculated lattice parameters being 2%–3% smaller than their experimental counterparts (Table I).

We start from the Gd intermetallics formed with IB group elements, namely GdCu, GdAg, and GdAu. For GdCu, in Ref. [40], it has been reported that at room temperature, the as-cast bulk samples of GdCu adopt a CsCl-type crystallographic structure, but when the temperature is lowered a martensitic structural transformation to FeB-type structure begins around 250 K continuing down to 120 K. After a thermal cycle through the forward and the reverse transformation, at room temperature the amounts of the phases present are $\sim 25\%$ for the CsCl-type structure and $\sim 75\%$ for the FeB-type structure. In contrast, in powdered samples the CsCl-type phase is stable at any temperature. The authors have observed that in the CsCl phase, an antiferromagnetic ordering sets in at $T_N = 150$ K, whilst a further magnetic transition happens in the FeB structure at $T_N = 45$ K [40]. As seen in Table I, we find AF-B order ($\mathbf{k} = [0\frac{1}{2}\frac{1}{2}]$) in the CsCl structure in agreement with experiment, although the calculated Néel temperature T_N of 45 K is substantially lower than the observed value. The calculated rate of the increase of the Néel temperature with pressure, $dT_N/dP = 0.02$ K kbar⁻¹, is, however, in fair agreement with experiments [41,42].

Moving on to GdAg, one can see in Table I that the reported experimentally measured Néel temperature lies between 132 and 155 K and the magnetic order is antiferromagnetic, common apparently to all the CsCl-structured rare-earth intermetallics with the group IB elements [4]. Our calculated order is also antiferromagnetic, of the AF-B type ($\mathbf{k} = [0\frac{1}{2}\frac{1}{2}]$), and the corresponding Néel temperature is 57 K which increases under pressure with the rate of 0.08 K kbar⁻¹, in qualitative agreement with measurements.

GdAu also appears to crystallize in the simple CsCl structure, although in some annealed samples transformations to the CrB structure were reported. Similarly to GdCu and GdAg, it exhibits an antiferromagnetic order, with the corresponding Néel temperature of 37 K. In the calculations, as already mentioned, we have only considered the CsCl structure

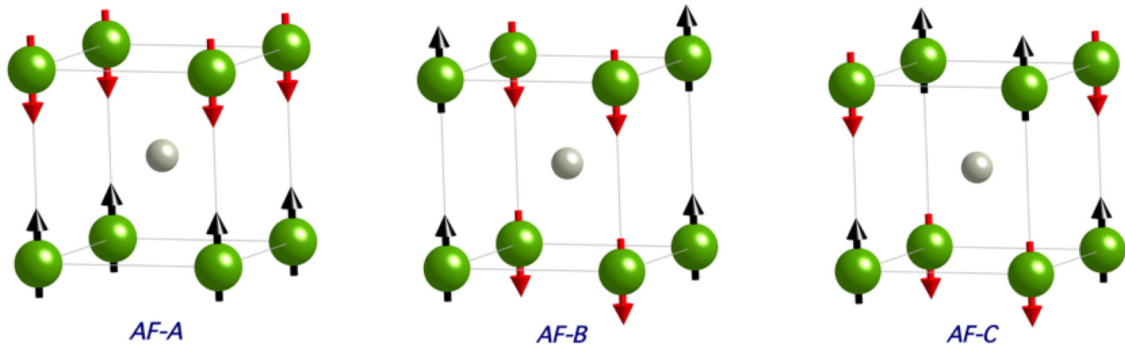


FIG. 1. The three possible antiferromagnetic orderings for the unit cell of the CsCl structured compounds. Here the green balls stand for the Gd atoms and the small, silverish, sphere in the center of the cubes defines the respective anions. The black and red arrows refer, respectively, to the local magnetic order parameter \mathbf{m}_i orientations pointing parallel or antiparallel to a one of the three fundamental translation vectors that define the cubic lattice.

for GdAu, and have found an antiferromagnetic order of the AF-B type, with the corresponding Néel temperature of 44 K comparing favorably with the experimental value [48].

The Gd-intermetallic compounds GdZn, GdCd, and GdHg, formed with the divalent group IIB elements, are isoelectronic with two s electrons on the outer shell. Whilst the CsCl structure has been experimentally confirmed for GdZn and GdCd, for GdHg it is less certain [2]. Under ambient conditions, GdZn and GdCd are ferromagnets with rather high Curie temperatures, respectively, $T_C = 270$ K for GdZn [6] and $T_C = 265$ K for GdCd [49]. We are not aware of the corresponding experimental data for GdHg. In our calculations, assuming the CsCl structure, we predict all three compounds to be ferromagnetic, and, as can be seen from Table I, with the predicted T_C and dT_C/dP in overall good agreement with experiment for both GdZn and GdCd [25,26]. Note that the dT_C/dP of GdZn is the only negative rate among all the compounds studied here, in rather satisfying qualitative agreement with available experimental evidence.

It may be useful to mention here that Rusz *et al.*, calculating the critical temperatures of GdX ($X=\text{Mg, Rh, Cd, Zn, Cu, Ag, Tl}$) intermetallics, within the Heisenberg Hamiltonian, using, respectively, the mean-field and random-phase approximations [53–55], noticed strong dependence of their results on the reference state for mapping on the exchange interactions and the choice of the atomic sphere radii. Their electronic structure calculations were performed using the linear muffin-tin orbital (LMTO) method within the atomic sphere approximation (ASA). They found that whilst GdAg and GdZn were generally well described, for the remaining compounds the predicted magnetic order and/or critical temperature depended on the details of the calculations. Buschow *et al.* [56], using modern mean-field theories and including spin-fluctuation effects by means of Mohn-Wohlfarth theory [57], estimated the critical temperature for GdZn of respectively 1060 and 410 K. In variance to the approaches used by Rusz *et al.* [54,55] and Buschow *et al.* [56], our *ab initio* modeling, providing an adequate description of the localized nature of the Gd $4f$ electron states, does not involve any mapping on a model Heisenberg Hamiltonian and does not make use of Mohn-Wohlfarth theory. In some earlier work, apart from predicting the magnetic correlations in GdZn and GdCd both at ambient temperature and under pressure, we were

also able to construct a magnetic phase diagram for GdMg, which included ferromagnetic, antiferromagnetic, and canted magnetic phases, highlighting a considerable deviation from the simple RKKY model [25]. Note that *ab initio* modeling of magnetic phase diagrams in magnetic metals, as was done for GdMg, requires not only pairwise but also higher-order interactions. Further details can be found in Refs. [30,31].

Among the Gd compounds with the trivalent group IIIA elements, GdGa crystallizes in the orthorhombic CrB structure. According to Ref. [14], GdGa orders ferromagnetically with the Curie temperature of $T_C = 200$ K. More recent calculations for GdGa in the true CrB structure confirm it to be ferromagnetic [58]. For GdIn, an early report of CsCl structure [39] was not confirmed by follow up measurements [5] and a tetragonal structure was suggested in Ref. [46]. GdTl is found to undergo a cubic to tetragonal structure transition around 300 K, with the cubic and tetragonal phases co-existing over a temperature range of 200 K. An antiferromagnetic transition is expected to occur below 200 K in the cubic phase. (Apparently GdTl_{0.9}Ag_{0.1} remains cubic down to 8 K, and has an antiferromagnetic transition temperature of 103 K [51]). In our calculations, for the sake of studying trends, we assume a CsCl unit cell for GdGa, GdIn, and GdTl, and find all three to be antiferromagnets characterized by the wave vector $\mathbf{k} = [00\frac{1}{2}]$, as seen in Table I. We predict Néel temperatures ranging from $T_N = 42$ to 98 K. Considering that for all the compounds in this group the calculations have been performed in the CsCl structure instead of the respective observed ones, the agreement with the available experiments is satisfactory. It should be noted that, according to our calculations, in the CsCl structure moderate pressures bring about a transition from antiferromagnetic to ferromagnetic order for both GdAu and GdTl.

The AF-B to F to AF-A sequence of magnetic orders that we have predicted here for GdCu-GdZn-GdGa, and again for GdAg-GdCd-GdIn and GdAu-GdHg-GdTl sets of ordered compounds, in agreement with the much earlier experimental work, is associated with the change in the number of conduction electrons from one to three across each of these sets. No change of magnetic structure is observed for the isoelectronic compounds of Gd within a given group of elements, e.g., GdCu, GdAg, and GdAu, confirming that it is indeed the number of conduction electrons, rather than the site separation, that plays a decisive role.

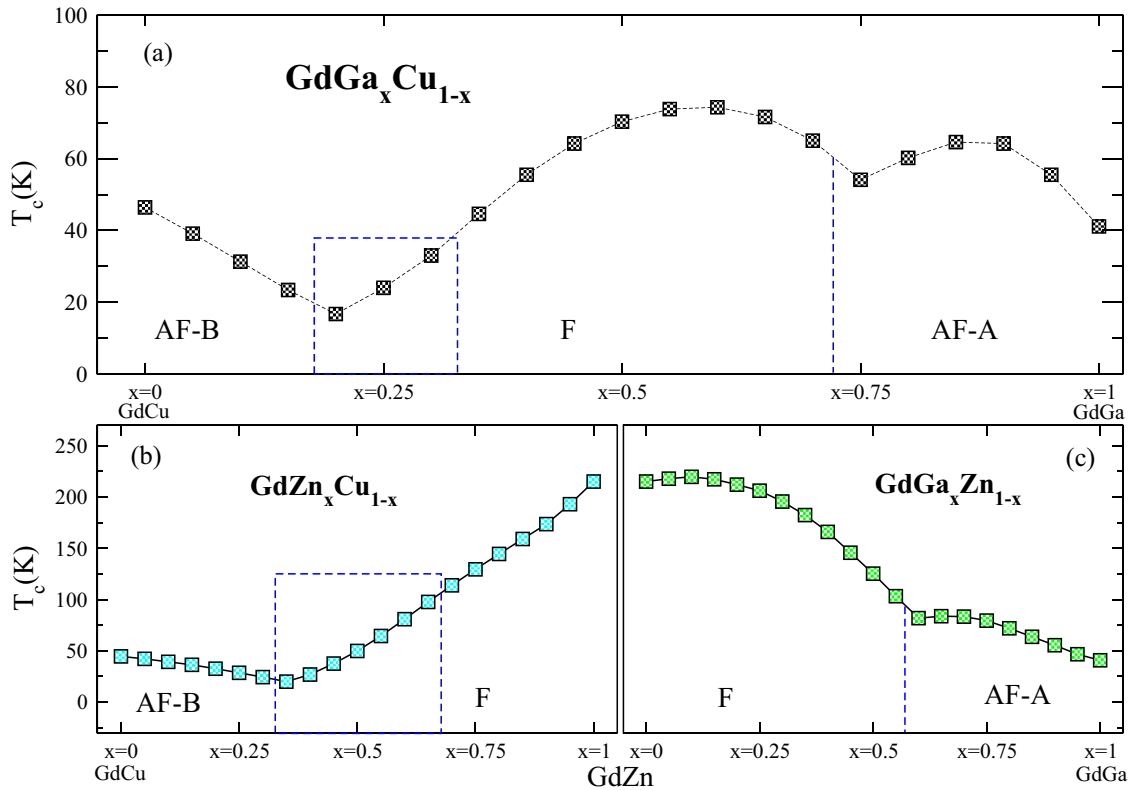


FIG. 2. The dependence of the calculated T_c on the anion concentration x for the alloys $\text{GdGa}_x\text{Cu}_{1-x}$ (a), $\text{GdZn}_x\text{Cu}_{1-x}$ (b), and $\text{GdGa}_x\text{Zn}_{1-x}$ (c). The different magnetic phases as a function of doping are indicated below the curves. The blue, dashed, boxes seen in (a) and (b) mark the regions of the incommensurate magnetic orders. The vertical dashed blue line in (a) and (c) indicates the boundary between F and AF-A phases.

IV. ALLOYS

Given that the methodology we use allows us to study systems with both magnetic and chemical disorder, in this section we concentrate on applying it to a number of random substitutional alloys, $\text{GdA}_x\text{B}_{1-x}$, i.e., solid solutions of the A and B anions discussed in the previous section. Specifically, we consider the $\text{GdZn}_x\text{Cu}_{1-x}$, $\text{GdCd}_x\text{Ag}_{1-x}$, $\text{GdZn}_x\text{Ag}_{1-x}$, $\text{GdGa}_x\text{Cu}_{1-x}$, $\text{GdGa}_x\text{Zn}_{1-x}$, $\text{GdIn}_x\text{Zn}_{1-x}$, $\text{GdIn}_x\text{Cd}_{1-x}$, and $\text{GdIn}_x\text{Ag}_{1-x}$ alloys. The aim is to shed some light on how continuous changes in the number of valence electrons and/or compositional disorder, through the resulting influence on the electronic structure, can impact on the development of long range magnetic order. This in turn should lead to a better understanding of what is mediating the exchange interactions between the $4f$ moments in these systems and whether it is the number of valence electrons or the site separations that play the more prominent role in establishing the resulting magnetic order. The calculated T_c 's associated with those magnetic orders of the studied alloys that we present in this section quantify the predominant magnetic correlations in the paramagnetic state.

Experimentally not all the alloys studied in this section can be synthesized in the CsCl structure, in particular those that contain either Ga or In constituent. For example, $\text{GdIn}_x\text{Ag}_{1-x}$ occurs in the CsCl structure for $x \leq 0.5$, but for the larger x concentrations the alloy appears to be in the tetragonal structure [46]. However, for the purpose of the calculations, where

we are mostly interested in studying trends as a function of the compositions of the alloys, we assume the CsCl structure for all the alloys. The lattice parameters of the different alloys are derived from Vegard's law [59] using the theoretical lattice parameters of the constituent pure compounds. Further technical details of the calculations are discussed in Appendix A.

Starting from the Gd alloys with the Cu/Zn/Ga series, in Fig. 2, the critical temperature as a function of an anion concentration x is presented for the three different alloys, $\text{GdGa}_x\text{Cu}_{1-x}$, $\text{GdZn}_x\text{Cu}_{1-x}$ and $\text{GdGa}_x\text{Zn}_{1-x}$. In $\text{GdGa}_x\text{Cu}_{1-x}$ [Fig. 2(a)], for $x = 0$, at the left-hand side of the graph, we deal with the pure GdCu system, exhibiting the AF-B type ($\mathbf{k} = [0\frac{1}{2}\frac{1}{2}]$) antiferromagnetic order, as discussed in the previous section. With the onset of Ga doping, the AF-B phase remains stable up to 20% concentration, where an incommensurate phase develops between 20% and 30% of Ga. The latter is characterized by the associated wave vector \mathbf{k} not corresponding to any symmetry point of the CsCl Brillouin zone (see Appendix A for details). From $x = 0.3$ onwards, ferromagnetic order sets in and remains the energetically most favorable phase up to around 75% Ga, where it is replaced by AF-A antiferromagnetic order ($\mathbf{k} = [00\frac{1}{2}]$), up to the pure GdGa compound. The $\text{GdZn}_x\text{Cu}_{1-x}$ alloy, depicted in Fig. 2(b), is characterized by two different magnetic orderings, respectively, antiferromagnetic (AF-B) for large concentrations of Cu, and ferromagnetic (F) for small Cu concentrations (i.e. close to the pure GdZn compound),

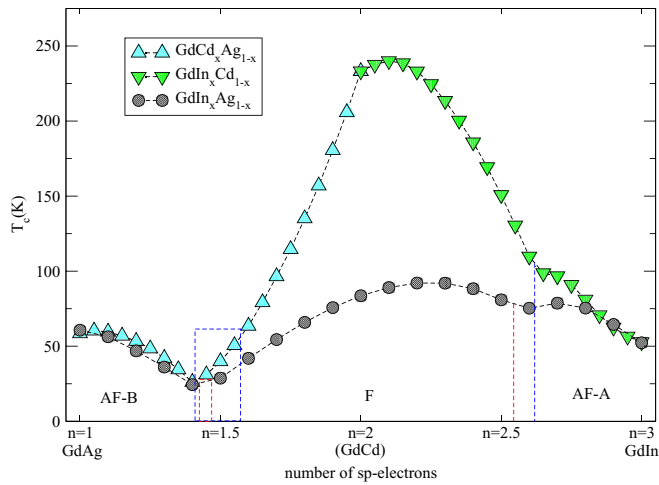


FIG. 3. The calculated T_c 's as a function of the number of sp electrons for $\text{GdCd}_x\text{Ag}_{1-x}$, $\text{GdIn}_x\text{Cd}_{1-x}$, and $\text{GdIn}_x\text{Ag}_{1-x}$ alloys. The blue and red dashed box enclose the areas with incommensurate magnetic order for respectively $\text{GdCd}_x\text{Ag}_{1-x}$ and $\text{GdIn}_x\text{Ag}_{1-x}$ alloys. The red and blue vertical dashed lines indicate the boundary between F and AF-A phases, respectively, for $\text{GdIn}_x\text{Ag}_{1-x}$ and $\text{GdIn}_x\text{Cd}_{1-x}$ alloys.

separated by a region of incommensurate ordering that ranges from around $x = 0.35$ to 0.7 . Finally, for the $\text{GdGa}_x\text{Zn}_{1-x}$ alloy, starting from the ferromagnetic GdZn , a straightforward transition to an antiferromagnetic phase (AF-A) occurs at 55% Ga, as can be seen in Fig. 2(c).

At first glance, it appears that whilst alloying two antiferromagnetic compounds, GdCu and GdGa , gives rise to a third, intermediate, ferromagnetic, phase over a wide range of Cu/Ga concentrations [Fig. 2(a)], only simple transitions occur in such alloys as $\text{GdZn}_x\text{Cu}_{1-x}$ [Fig. 2(b)] and $\text{GdGa}_x\text{Zn}_{1-x}$ [Fig. 2(c)] that are solid solutions of a ferromagnetic and an antiferromagnetic component. However, when comparing the overall dependence of T_c on concentration in Fig. 2(a) to that observed in Figs. 2(b) and 2(c) combined, one sees a very similar sequence of crests and valleys, including the transition region characterized by an incommensurate ordering. The ordered compounds GdCu and GdGa differ by two sp electrons in the outer shell, and within the CsCl structure, assuming a rigid band picture, for the $\text{GdGa}_{0.5}\text{Cu}_{0.5}$ alloy, one would expect an electronic structure similar to the GdZn compound. This is in line with the fact that at 50% Cu concentration, the alloy is ferromagnetic as is the case for GdZn in Figs. 2(b) and 2(c). Within the Cu/Zn/Ga alloy series, the change in magnetic ordering appears to be driven by the number of sp electrons, rather than by the anions involved, although quantitatively the observed T_c depends on the constituent chemistry.

A similar picture emerges for the Gd-alloys with the 4d Ag/Cd/In series in Fig. 3 where, rather than the dependence on the anion concentration x , we have plotted the variation of T_c and T_N as a function of the number n of the 5 sp electrons in the $\text{GdIn}_x\text{Ag}_{1-x}$, $\text{GdCd}_x\text{Ag}_{1-x}$, and $\text{GdIn}_x\text{Cd}_{1-x}$ alloys; the latter two being combined in a single graph. GdAg ($n = 1$) and GdIn ($n = 3$) differ by two valence electrons, and gradually increasing n from one to three leads to a sequence

of changes in magnetic ordering from AF-B to incommensurate to ferromagnetic (F) to AF-A. The observed variation is qualitatively very similar, regardless whether we consider the combined graphs $\text{GdCd}_x\text{Ag}_{1-x}$ and $\text{GdIn}_x\text{Cd}_{1-x}$, where n changes in steps of one electron, or $\text{GdIn}_x\text{Ag}_{1-x}$, where GdAg and GdIn differ by two electrons. The observed magnetic order and variation in T_c around $n = 2$ indicate a very similar electronic structure for GdCd and $\text{GdIn}_{0.5}\text{Ag}_{0.5}$, as would be expected in the rigid band-picture proposed earlier for $\text{GdGa}_x\text{Cu}_{1-x}$. The calculated T_c 's for the two graphs differ in absolute terms (by more than 100% around $n = 2$), indicating that the quantitative properties depend on the physical and chemical characteristics of the constituents of the specific alloys. In that respect, one noticeable difference between $\text{GdIn}_{0.5}\text{Ag}_{0.5}$ and GdCd is the increased degree of localization of the 4d states in In compared to Cd, which results in decreased hybridization with the Gd 5d states thus affecting the density of states (DOS) at the Fermi level.

To gain some insight on whether atom separation may influence transition temperatures and the exchange interactions we have also studied the $\text{GdCu}_x\text{Ag}_{1-x}$ alloy, where Cu and Ag have the same number of conduction electrons, i.e., they are isoelectronic, but Ag being a 4d electron element has a larger atomic radius (1.445 Å for coordination number (CN) of 12) compared to the 3d electron element Cu (atomic radius is 1.252 Å for CN=12). What we find is that starting from the ordered GdCu compound, and alloying it with Ag, does not change the antiferromagnetic order which remains uniformly AF-B for all the alloy concentrations, whilst the Néel temperature gradually increases by up to 20%, when reaching the pure GdAg compound. This result supports our findings above that it is the change in the number of conduction electrons, and not the separation between atoms, that drives the observed changes in the nature of the magnetic transitions in the studied Gd intermetallics alloys.

In order to assess the adequacy of our theory, in Fig. 4, we compare the calculated and experimentally observed critical temperatures of the Gd-Ag/Zn/In series of alloys. Starting with $\text{GdZn}_x\text{Ag}_{1-x}$, we notice an overall rather good qualitative agreement for the observed trend as a function of Zn concentration, both in the antiferromagnetic ($x < 0.4$) and ferromagnetic ($x > 0.7$) regions. Whilst the transition between these two magnetic regimes in our calculations is characterized by an incommensurate ordering (open squares), ranging from $0.4 < x < 0.7$, in the experimental results by Koebler *et al.* [13,60], the same region displays a complicated mixture of coexisting magnetic phases (not shown here).

For $\text{GdIn}_x\text{Zn}_{1-x}$, the experimentally observed ferromagnetic to antiferromagnetic transition as a function of In doping is overall well reproduced by our calculations, although only a few experimental data points exist for high In concentrations. Beyond the transition point, in the antiferromagnetic region, a couple of measurements appear to confirm the decreasing trend in T_c observed in our calculations, which however should be interpreted with care, given that there exists some uncertainty regarding the stable crystal structure of GdIn . Noticeably, we find a discrepancy between theory and experiment for small concentrations of In below $x = 0.2$. Whilst the results by both Alfieri *et al.* [10] and Hiraoka *et al.* [61] indicate a smoothly decreasing critical temperature,

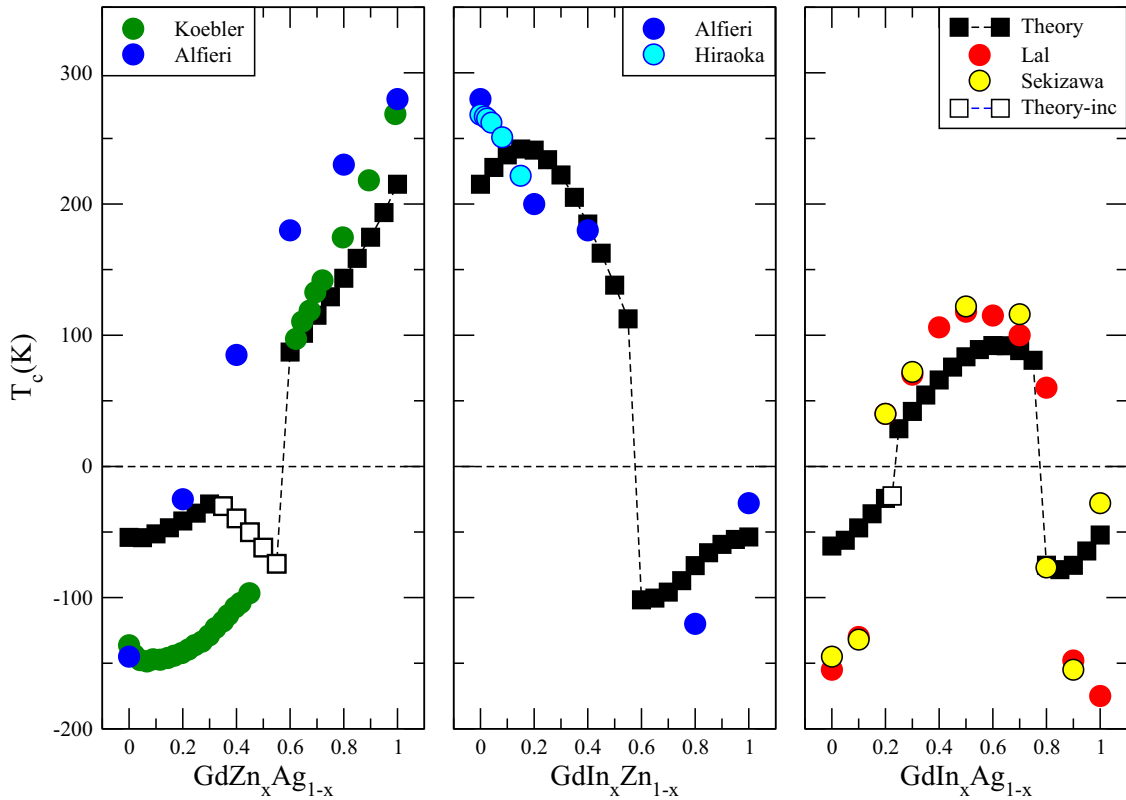


FIG. 4. A comparison of theory and experiment for critical temperatures T_c as a function of alloying concentration x for $\text{GdZn}_x\text{Ag}_{1-x}$, $\text{GdIn}_x\text{Zn}_{1-x}$, and $\text{GdIn}_x\text{Ag}_{1-x}$. Here the positive temperatures refer to the ferromagnetic order, while the transition temperatures corresponding to the antiferromagnetic and incommensurate orders are plotted on the negative side of the temperature axis.

our calculations find initially an increase in T_c , for $x < 0.2$, followed by a decrease from 0.2 onwards. For $\text{GdIn}_x\text{Ag}_{1-x}$, the agreement with experiment is very good, both qualitatively in terms of the Ag concentrations where the ferro-antiferro transitions around $x = 0.3$ and 0.8 occur, as well as quantitatively, specifically in the ferromagnetic region.

The increase in T_c that we calculate as a function of small dopant concentrations x in $\text{GdIn}_x\text{Zn}_{1-x}$, we also predict when adding small concentrations of Ga to GdZn [Fig. 2(c)] and In to GdCd (Fig. 3). Since, for the latter two alloys no experimental data could be found to check against, we have performed measurements for $\text{GdGa}_x\text{Zn}_{1-x}$ at small Ga concentrations and compare them to our calculations in Fig. 5. Details of the measurements are discussed in Appendix B. We observe that the calculated T_c (open squares) increases, albeit rather weakly, up to $x = 0.1$ at which point it starts decreasing rapidly, whilst experiment (orange circles) shows a decreasing T_c for all measured concentrations. Qualitatively the discrepancy between theory and experiment is thus very similar to that observed in $\text{GdIn}_x\text{Zn}_{1-x}$ (Fig. 4), and it is unclear what is the cause of it. In the calculations, atomic relaxation when gradually replacing Zn with In or Ga is not accounted for by a corresponding change in MT radii (see Appendix A), an approximation that might be less justified for In which has a rather large atomic radius of 1.666 Å for CN=12, compared to 1.394 Å for Zn, than for Ga with rather similar atomic radius of 1.353 Å. This could be the reason why in $\text{GdGa}_x\text{Zn}_{1-x}$ T_c increases rather moderately, by 5 K, before starting to decrease around $x = 0.1$, whilst in $\text{GdIn}_x\text{Zn}_{1-x}$ the

observed increase in T_c is 25 K, starting to decrease at $x = 0.15$. However, even taking this size difference into account, the overall discrepancy remains, and one of the possible reasons may be that the calculations assume ideally disordered alloys, while the samples used in experiments may not be uniformly so, particularly at such small concentrations. Apart from the above discussed discrepancy, it emerges that the overall, both qualitative and quantitative, agreement between the theoretical and experimental results is very good and gives us confidence that the underlying theory of the method used, both in terms of the *ab initio* treatment of the localized nature of the Gd 4*f* electron states, as well as, the magnetic and chemical disorders, takes into account all the important physical characteristics of the studied systems.

V. DISCUSSION AND ANALYSIS OF RESULTS

It is generally accepted that the very localized character of the rare-earth 4*f* electrons implies that the ordering of the corresponding spin moments happens through indirect exchange coupling. From the preceding sections it emerges that our first-principles methodology, i.e., the SIC-LSDA combined with the DLM and CPA approaches, is capable of predicting the magnetic ordering of both the ordered compounds and intermetallic binary alloys to a high degree of accuracy, as testified in particular by Fig. 4, showing an overall good agreement between calculations and experiments. The question now arises whether, based on these findings, we are in a position to identify the underlying mechanism mediating the

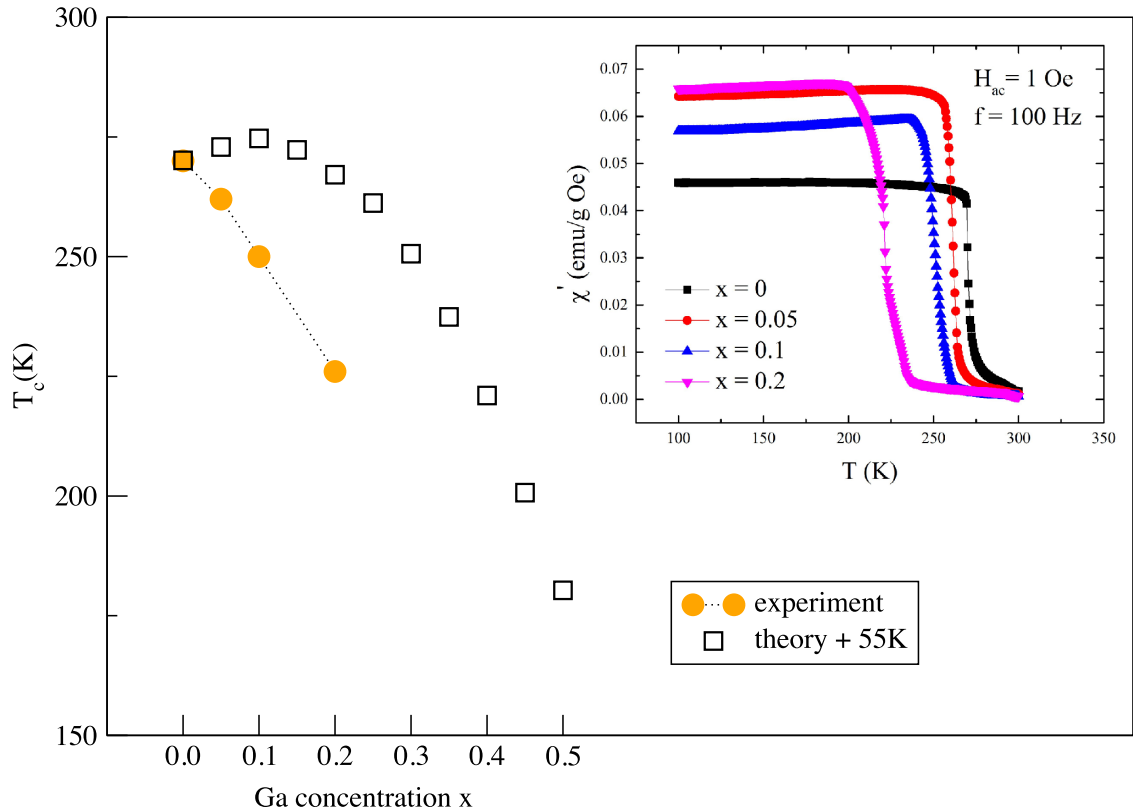


FIG. 5. A comparison of the calculated and measured T_c 's of $\text{GdGa}_x\text{Zn}_{1-x}$ alloys. The calculated values are shifted by 55 K upwards to align the measured and calculated transition temperatures for $x = 0$, so that the slopes of the respective curves can be better compared. The inset shows the real part of ac magnetic susceptibility measured as a function of temperature for the four examined Ga concentrations x , from which the respective T_c 's have been extracted.

exchange interaction between the Gd $4f$ moments and thus also the driving force behind the observed variation in T_c as a function of concentration.

As mentioned earlier, two different mechanisms have been proposed for this indirect exchange coupling. In the case of RKKY [8], this happens through the intermediary of the s -conduction electrons that locally couple to the $4f$ electrons, which results in the effective interaction whose strength decays as R^{-3} and for large R is proportional to $\cos(2k_F R)$, oscillating between ferromagnetic and antiferromagnetic orderings as a function of R . For free electrons, $k_F = (3\pi^2 n)^{1/3}$, and thus is directly related to the density of conduction electrons n . Despite its approximations, the simplified RKKY interaction captures the magnetic properties of rare-earth compounds in many cases [62], although there tend to be noticeable deviations from the predicted behavior that require a more exact treatment of the actual band character of the conduction electrons [25,62].

An alternative mechanism suggested by Campbell [9], is based on the local exchange interaction of the $4f$ electrons on the rare-earth ions with their corresponding $5d$ electrons, and mediated by the direct overlap of these d -electron states on neighboring sites. It could be acting as a competing (ferromagnetic) mechanism for magnetic ordering in compounds where the rare-earth nearest-neighbor ions are close. From their LSDA based electronic structure calculations on GdZn, Postnikov *et al.* [63] observed the

DOS at the Fermi level to be strongly influenced by the Gd $5d$ states, and conjectured the ferromagnetic ordering in GdZn to be stabilized by the relatively low DOS at the Fermi level. No specific exchange mechanism was proposed. In their LMTO calculation, treating the $4f$ electrons as part of the core, Buschow *et al.* [56] similarly observed that DOS at the Fermi level was characterized by Gd $5d$ -electron states, with almost no presence of the s -electron states, which made the authors conclude that an fd -exchange combined with a $d-d$ interaction was the mechanism for the indirect exchange coupling in these materials, rather than the RKKY interaction that requires delocalized s electrons. Our recent calculations for, respectively, GdZn, GdCd, and GdMg, under pressure, have shown that the valence electron glue in which the $4f$ moments sit also can provide deviations from the RKKY [25]. Its spd electrons can shift it far from a nearly free electron model, as exemplified by the canted magnetism of GdMg and the stark contrast of the magnetism of isoelectronic GdZn and GdCd with their disparate pressure variations [25].

From our present calculations for both the $3d$ and $4d$ ordered compounds, the overall change in magnetic ordering from antiferromagnetic to ferromagnetic and again to antiferromagnetic, as a function of the density of sp electrons, would appear to have features in common with what a RKKY interaction would produce, although the more complex valence electronic structures that these compounds have leads to

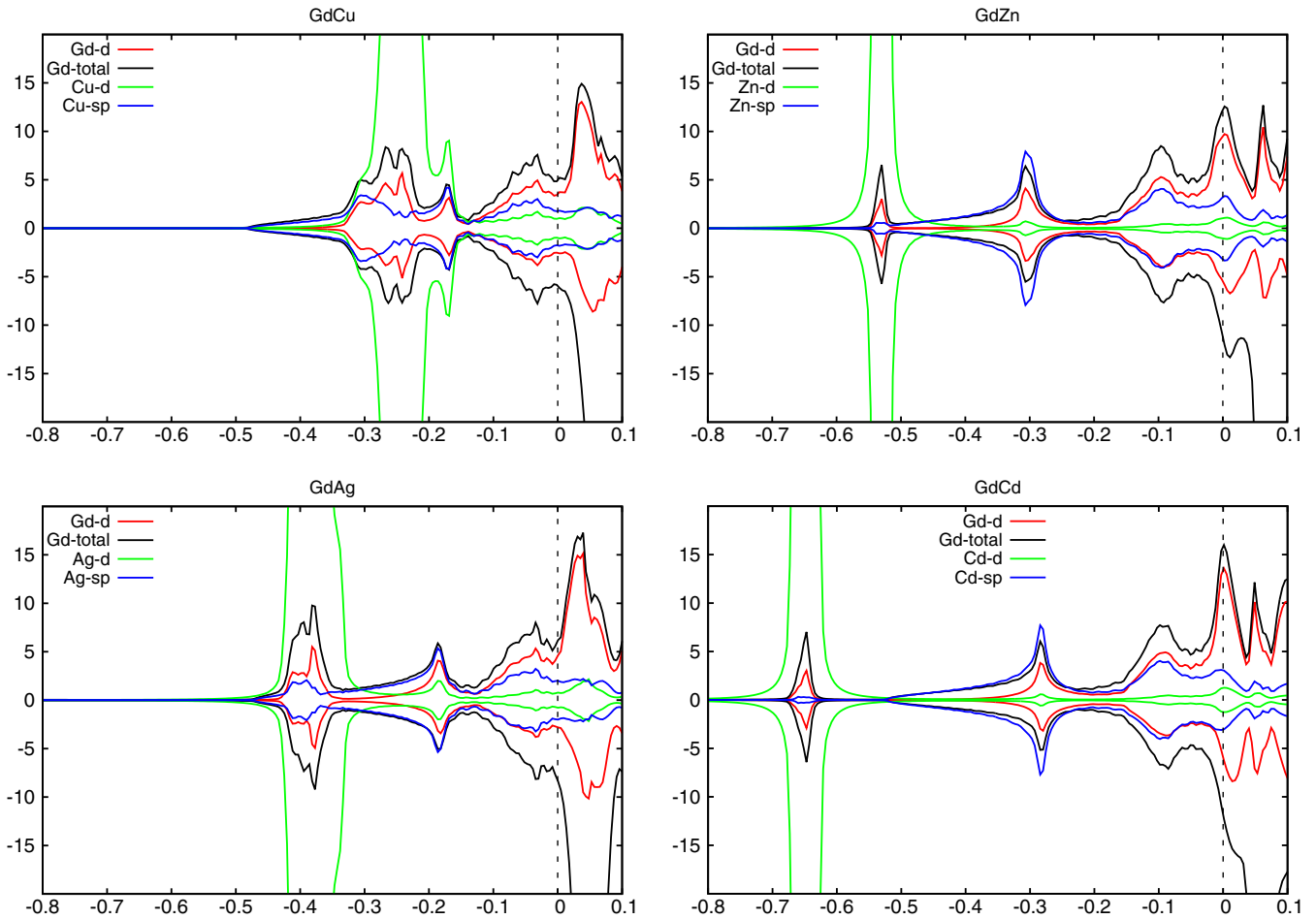


FIG. 6. The local densities of states (DOS) (in states/Ry cell), as functions of energy (in Ry), calculated within DLM, respectively, for GdCu (top left), GdZn (top right), GdAg (bottom left), and GdCd (bottom right). The total Gd contribution (black curve) and its d -electron component (red curve) are shown, as are also the anion sp - (blue curve) and d -electron (green curve) components. The DOS for an electron spin-polarized parallel (antiparallel) to the local moment on the Gd site is shown on the positive (negative) side of the y axis. The total DOS, an average over all directions, is unpolarized. The localized Gd $4f$ states for each compound are located at ~ -1.2 Ry, but are not shown here. The vertical dashed black lines indicate the position of the Fermi level.

important deviations from this simple model. From Figs. 2 and 3, we notice that there is an incommensurate phase which only occurs in the early parts of the phase diagram where the number of sp electrons remains below two. In the second half, i.e., for $n > 2$, the magnetic ordering changes directly from ferromagnetic to antiferromagnetic without a transition through an incommensurate region. A possible explanation can be derived from the densities of states of the respective pure compounds constituting a given alloy, displayed in Fig. 6. We observe that when moving from GdCu (top left) to GdZn (top right), the anion $3d$ peak shifts towards higher binding energies (increased localization). For GdGa (not shown), this peak is situated at -1 Ry, i.e., almost corelike. From GdCu to GdGa, with the growing number of anion sp electrons resulting in the filling up of the corresponding d states, the latter become increasingly localized, and less inclined to hybridize with the Gd d states. Assuming that hybridization produces non-RKKY like exchange interactions, we would expect them to be most noticeable in alloys containing a high concentration of anions with delocalized d states. Interestingly, it is in these same alloys that the incommensurate transition regions are

observed, indicating that these are associated with complex magnetic interactions mediated by the Gd $5d$ states hybridizing with anion d states. Conversely, in alloys containing a high concentration of anions with localized d states, this hybridization with the Gd $5d$ states does not occur, and correspondingly the magnetic phase diagram, relying solely on interactions mediated by anion sp and Gd $5d$ states, does not involve an incommensurate region. For the $4d$ series, a similar trend of increased localization is observed from GdAg (bottom left) to GdCd (bottom right) and GdIn (not shown), and also here the incommensurate region observed for $\text{GdCd}_x\text{Ag}_{1-x}$ can be associated with the Gd $5d$ states hybridizing with the anion d states. Furthermore, comparing the $3d$ and $4d$ series in Fig. 6, it emerges that the $4d$ peaks are situated at higher binding energies than their $3d$ counterparts. Our calculated DOS for GdCu and GdAg agree qualitatively with XPS measurements of the respective valence-band structures [64]. These different degrees of localization appear to be reflected in the range of the corresponding incommensurate regions, as the largest range is observed in Fig. 2 for the alloys composed of the $3d$ elements.

VI. CONCLUSIONS

We have presented first-principles results for the magnetic properties of a number of equiatomic Gd intermetallic compounds that adopt CsCl-type structure and their alloys, based on the combined DLM + CPA + SIC approach, implemented within the SCF-KKR-CPA method. Specifically, we have considered GdX intermetallics with the elements of IB, IIB, and IIIA groups. Among the alloys, we have studied in detail the GdCu/Zn/Ga and GdAg/Cd/In series, facilitated by the CPA extension of our method. The most important outcome of these studies is the observation of an incommensurate phase for a number of alloys, providing a considerable deviation from the RKKY-like “AF-B to F to AF-A” sequence of magnetic orders, governed by the change in the number of the conduction electrons within a given series. From inspecting the calculated densities of states we have been able to identify the importance of d electron states for mediating exchange interactions among the $4f$ localized moments of Gd. In particular, the degree of Gd $5d$ hybridization with the d electron states of the anion constituents appears to control the occurrence of the incommensurate phases in some of the studied alloys. Furthermore, the overall good agreement with experiments provides full support to the methodology we use for studying magnetic correlations in the paramagnetic state and the magnetic orders they give rise to for the systems studied here and many future applications.

ACKNOWLEDGMENTS

The work was supported by the United Kingdom EPSRC by Grants No. EP/J006750/1 and No. EP/M028941/1 and an EPSRC service level agreement CoSeC with the Scientific Computing Department of STFC. Work at Ames Laboratory was supported by the Materials Sciences and Engineering Division of the Office of Basic Energy Sciences of the U.S. Department of Energy under Contract No. DE-AC02-07CH11358 with Iowa State University.

APPENDIX A: TECHNICAL DETAILS

1. Muffin-tin radii

Here we discuss some technical details of the calculations, specifically the dependence of the transition temperatures on the choice of the MT radii in the alloy calculations. Starting from binary compounds each having a specific set of anion and Gd MT radii, a choice has to be made for the respective MT radii of the corresponding alloys. One possibility is to use an average over the constituent binary compounds, as was done for $\text{GdCd}_x\text{Ag}_{1-x}$ (red open circles) in Fig. 7, where the MT radii used are those obtained from averaging over the corresponding radii of GdAg and GdCd. Similarly for $\text{GdCd}_x\text{In}_{1-x}$ in Fig. 7 (blue open circles), where the average is over the MT radii of GdCd and GdIn. Noticeably, at GdCd these two curves do disagree, highlighting the dependence of T_c on the choice of MT radii. An alternative to using average MT radii is indicated by the curve outlined by triangles, where the MT radii of the pure GdCd compound have been applied for all concentrations of $\text{GdCd}_x\text{Ag}_{1-x}$ (left triangles) and $\text{GdCd}_x\text{In}_{1-x}$ (right triangles). Comparing the different curves,

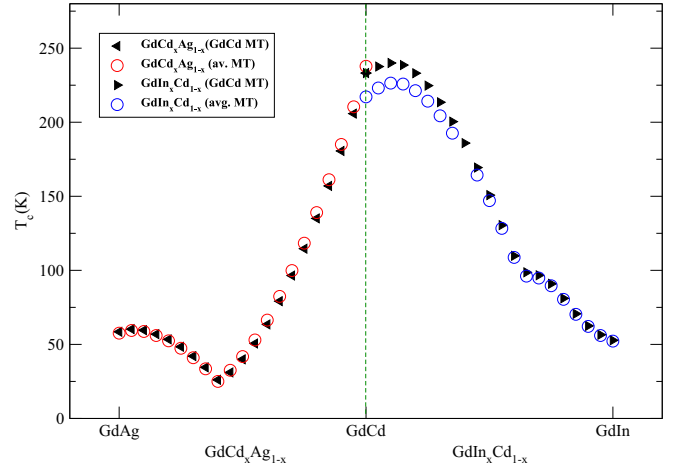


FIG. 7. The dependence of T_c on the choice of the Gd and anion MT radii, along the path starting from the pure GdAg compound, through the $\text{GdCd}_x\text{Ag}_{1-x}$ alloy, by gradually mixing in Cd, and then from the ordered GdCd compound, through the $\text{GdIn}_x\text{Cd}_{1-x}$ alloy, to the pure GdIn compound, by alloying GdCd with In. As described in the legend, the curves associated respectively with red and blue symbols refer to using MT radii obtained by averaging over the MT radii of the anion constituents involved in a given alloy. The Gd MT radii for the respective red and blue symbols are obtained by averaging over the Gd MT radii of the respective binary compounds, namely, GdAg and GdCd for the red symbols curve, and the Gd MT radii of GdCd and GdIn for the blue symbols curve. The black symbols relate to the calculations where the anion MT radius used throughout is the one of the divalent constituent, Cd in this case, while the Gd MT radius is that of Gd in the GdCd binary compound. The black asterisk marks the true transition temperature of the pure GdCd compound.

we can see that the choice of the MT radii does not affect much the antiferromagnetic order, as far as the value of the Néel temperature of GdAg and GdIn is concerned, but the transition temperature T_c , associated with the ferromagnetic order at GdCd is rather sensitive to the size of the MT radii. As a result, in order to best reproduce the T_c of the alloying components in the stoichiometric limit, and to consequently avoid the discontinuity at GdCd, we decided to use the GdCd-MT throughout, when alloying with either Ag or In (as was done in Fig. 3). Exactly the same procedure of choosing MT radii was applied for the alloys containing Zn, where a similar AF-F-AF crossover occurs as a function of Ag/In (Fig. 4) or Cu/Ga (Fig. 2) concentration. Notice that for alloys not containing Cd or Zn, e.g., $\text{GdIn}_x\text{Ag}_{1-x}$ or $\text{GdGa}_x\text{Cu}_{1-x}$, the averaging over constituent MT radii was used.

2. $S^{(2)}$ and magnetic order

In this section, we briefly explain how, based on $S^{(2)}(\mathbf{q}, T)$ [Eq. (A1)], the magnetically ordered, as well as incommensurate, regions and wave vectors are identified. $S^{(2)}(\mathbf{q}, T)$ has the following form [29,65,66]:

$$S^{(2)}(\mathbf{q}, T) \propto \iiint \frac{f(\epsilon) - f(\epsilon')}{(\epsilon - \epsilon')} A_B(\mathbf{k}, \epsilon) A_B(\mathbf{k} + \mathbf{q}, \epsilon') \times d\mathbf{k} d\epsilon d\epsilon', \quad (\text{A1})$$

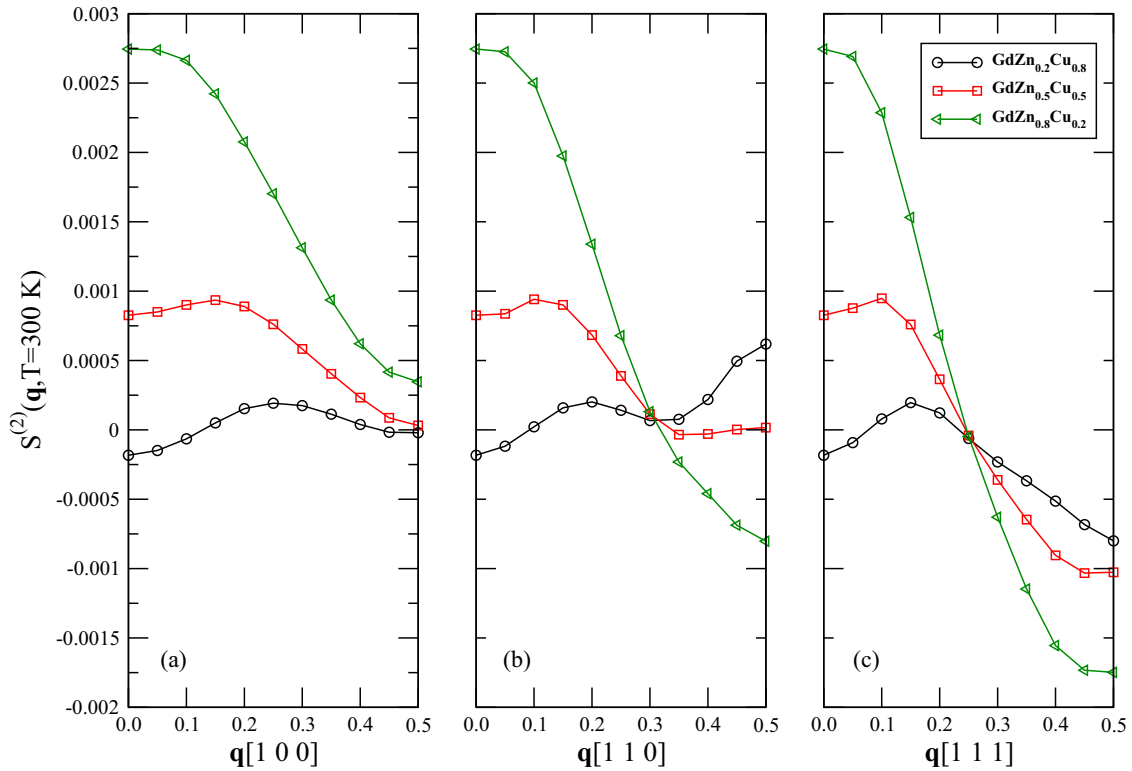


FIG. 8. The calculated lattice Fourier transform, $S^{(2)}(\mathbf{q}, T)$ [in Ry], of $\text{GdZn}_x\text{Cu}_{1-x}$ at $T = 300\text{K}$, for \mathbf{q} (in units of $\frac{2\pi}{a}$): (a) from $(0; 0; 0)$ to $(\frac{1}{2}; 0; 0)$, (b) from $(0; 0; 0)$ to $(\frac{1}{2}; \frac{1}{2}; 0)$, and (c) from $(0; 0; 0)$ to $(\frac{1}{2}; \frac{1}{2}; \frac{1}{2})$. The observed maxima are respectively for $\text{GdZn}_{0.8}\text{Cu}_{0.2}$ (green triangles) at $\mathbf{q}=(0,0,0)$, for $\text{GdZn}_{0.2}\text{Cu}_{0.8}$ (black circles) at $\mathbf{q}=(\frac{1}{2}, \frac{1}{2}, 0)$, and for $\text{GdZn}_{0.5}\text{Cu}_{0.5}$ (red squares) at $\mathbf{q}=(0.1, 0.1, 0.1)$.

where $A_B(\mathbf{k}, \epsilon)$ is the valence electron Bloch spectral function at wave-vector \mathbf{k} and energy ϵ , and $f(\epsilon)$ is the Fermi-Dirac function $\frac{1}{e^{\epsilon-\epsilon_F}/k_B T + 1}$. In Fig. 8, the calculated $S^{(2)}(\mathbf{q}, T)$ of the $\text{GdZn}_x\text{Cu}_{1-x}$ alloy is presented for three different concentrations x , and with \mathbf{q} along the three relevant symmetry directions of the CsCl Brillouin zone. For any given alloy concentration, the maximum of $S^{(2)}(\mathbf{q}, T)$ determines the associated magnetic order and \mathbf{q} vector. Namely, for the Zn-rich alloy, $\text{GdZn}_{0.8}\text{Cu}_{0.2}$, the maximum is at $\mathbf{q}=(0,0,0)$ corresponding to a ferromagnetic order. For the Cu-rich alloy, $\text{GdZn}_{0.2}\text{Cu}_{0.8}$, the maximum is at $\mathbf{q}=(\frac{1}{2}, \frac{1}{2}, 0)$ associated with an antiferromagnetic order. For $\text{GdZn}_{0.5}\text{Cu}_{0.5}$, the maximum of the susceptibility is at $\mathbf{q}=(0.1, 0.1, 0.1)$, corresponding to an incommensurate order. Going through all concentrations x of a given alloy and scanning all the \mathbf{q} values along the three directions allows one to determine the whole magnetic phase diagram.

APPENDIX B: EXPERIMENTAL METHODS AND RESULTS FOR $\text{GdGa}_x\text{Zn}_{1-x}$

1. Experimental methods

A series of $\text{GdGa}_x\text{Zn}_{1-x}$ alloys ($x = 0, 0.05, 0.1, 0.2$) was prepared by melting the constituent metals in the high frequency induction furnace at 1670 K. Zn and Ga metals were at least 99.99 at. % pure (purchased from Alfa Aesar) and Gd (99.8 at. % with respect to all elements, including O, C, and N) was provided by Materials Preparation Center of Ames Laboratory. The stoichiometric amounts of constituent

elements were sealed under a purified He atmosphere in tantalum crucibles, which were heated in the vacuum inside the induction furnace. After melting, the samples were removed from the crucibles and annealed at 970 K for five days inside He filled quartz tubes. The crystal structure of the obtained samples was determined by the room temperature x-ray powder diffraction (XRD) using a Rigaku TTRAX powder diffractometer with Mo- K_α x-ray source and the full profile fitting Rietveld refinement of the powder diffraction patterns was performed using the program FULLPROF. To verify the actual chemical composition of the prepared alloys the energy dispersive spectroscopy (EDS) measurements were carried out on an FEI Teneo SEM equipped with an Oxford Instruments Aztec EDS system. A SQUID magnetometer (MPMS XL-7 by Quantum Design) was used to measure magnetic properties. The temperature dependence of magnetization was obtained in the presence of 2 kOe applied dc magnetic field during both cooling and heating. The ac-magnetic susceptibility measurements were performed in ac magnetic field with 1 Oe amplitude and 100 Hz frequency.

2. Experimental results and comparison with calculations

The XRD study reveals that all the samples form with the CsCl type cubic crystal structure. The lattice parameter a of the samples calculated from XRD data does not change with x within experimental errors (see Table II). At the same time, the EDS study confirms that the nominal and actual compositions of the prepared alloys are practically the same. The magnetization measurements indicate that all the samples

TABLE II. Lattice parameter a and the characteristic magnetic temperatures: the critical temperature T_c and the Weiss temperature θ_p of annealed $\text{GdGa}_x\text{Zn}_{1-x}$ alloys for the compositions $x = 0, 0.05, 0.1$, and 0.2 .

x	a (Å)	T_c (K)	θ_p (K)
0	3.5993 (± 0.0003)	270	266
0.05	3.5987 (± 0.0004)	262	254
0.1	3.5992 (± 0.0004)	250	241
0.2	3.6001 (± 0.0004)	226	200

exhibit similar magnetic behavior. Namely, a conventional magnetic transition from the high-temperature paramagnetic

phase to the low-temperature ferromagnetic phase is observed upon cooling. The transition temperature T_c is determined as the temperature corresponding to the fastest change in ac magnetic susceptibility, i.e., the temperature at which $d\chi'/dT$ (see the inset of Fig. 5) is minimum. The obtained T_c values are also listed in Table II.

The transition temperature T_c gradually decreases with the increase of Ga concentration, resembling the compositional dependence of the magnetic ordering temperature in the $\text{GdIn}_x\text{Zn}_{1-x}$ alloys [61]. The T_c of GdZn closely matches the value reported in literature. Above T_c , $H/M(T)$ measured in 2-kOe magnetic field follows Curie-Weiss law, from which Weiss temperature (θ_p) was also calculated, with the relevant values being close to T_c 's of the studied samples (see Table II).

- [1] J. W. Cable, W. C. Koehler, and E. O. Wollan, *Phys. Rev.* **136**, A240 (1964).
- [2] A. Iandelli and A. Palenzona, *J. Less-Common Metals* **9**, 1 (1965).
- [3] J. Pierre and R. Pauthenet, *CR ACAD. Sci. (France)* **260**, 2739 (1965).
- [4] J. W. Cable, W. C. Koehler, and H. R. Child, *J. Appl. Phys.* **36**, 1096 (1965).
- [5] K. Sekizawa and K. Yasukochi, *J. Phys. Soc. Jpn.* **21**, 684 (1966).
- [6] K. Kanematsu, G. T. Alfieri, and E. Banks, *J. Phys. Soc. Jpn.* **26**, 244 (1969).
- [7] A. Oppelt, E. Dormann, and K. H. J. Buschow, *Phys. Stat. Sol. B* **51**, 275 (1972).
- [8] T. Kasuya, *Prog. Theo. Phys.* **16**, 45 (1956).
- [9] I. A. Campbell, *J. Phys. F: Metal. Phys.* **2**, L47 (1972).
- [10] G. T. Alfieri, E. Banks, and K. Kanematsu, *J. Appl. Phys.* **37**, 1254 (1966).
- [11] K. Takei, Y. Ishikawa, N. Watanabe, and K. Tajima, *J. Phys. Soc. Jpn.* **47**, 88 (1979).
- [12] T. Yashiro, Y. Hamaguchi, and H. Watanabe, *J. Phys. Soc. Jpn.* **40**, 63 (1976).
- [13] U. Köbler, W. Kinzel, and W. Zinn, *J. Magn. Magn. Mater.* **25**, 124 (1981).
- [14] K. H. J. Buschow and W. W. van der Hoogenhof, *J. Less-Common Metals* **45**, 309 (1976).
- [15] J. Sakurai, Y. Kubo, T. Kondo, J. Pierre, and E. F. Bertaut, *Journal of Physics and Chemistry of Solids* **34**, 1305 (1973).
- [16] B. L. Gyorffy, A. J. Pindor, J. B. Staunton, G. M. Stocks, and H. Winter, *J. Phys. F: Met. Phys.* **15**, 1337 (1985).
- [17] J. P. Perdew and A. Zunger, *Phys. Rev. B* **23**, 5048 (1981).
- [18] L. Petit, R. Tyer, Z. Szotek, W. M. Temmerman, and A. Svane, *New J. Phys.* **12**, 113041 (2010).
- [19] W. M. Temmerman, L. Petit, A. Svane, Z. Szotek, M. Lüders, P. Strange, J. B. Staunton, I. D. Hughes, and B. L. Gyorffy, in *Handbook on the Physics and Chemistry of Rare Earths*, edited by K. A. Gschneidner, J. C. G. Bünnzli, and V. K. Pecharsky (North-Holland, Amsterdam, 2009), Vol. 39, Chap. 241, p. 1.
- [20] V. I. Anisimov, J. Zaanen, and O. K. Andersen, *Phys. Rev. B* **44**, 943 (1991).
- [21] S. L. Dudarev, G. A. Botton, S. Y. Savrasov, Z. Szotek, W. M. Temmerman, and A. P. Sutton, *Phys. Stat. Sol. A* **166**, 429 (1998).
- [22] M. Cococcioni and S. de Gironcoli, *Phys. Rev. B* **71**, 035105 (2005).
- [23] F. Aryasetiawan, K. Karlsson, O. Jepsen, and U. Schönberger, *Phys. Rev. B* **74**, 125106 (2006).
- [24] P. Soven, *Phys. Rev.* **156**, 809 (1967).
- [25] L. Petit, D. Paudyal, Y. Mudryk, K. A. Gschneidner, Jr., V. K. Pecharsky, M. Lüders, Z. Szotek, R. Banerjee, and J. B. Staunton, *Phys. Rev. Lett.* **115**, 207201 (2015).
- [26] L. Petit, Z. Szotek, J. Jackson, M. Lüders, D. Paudyal, Y. Mudryk, V. K. Pecharsky, K. A. Gschneidner, Jr., and J. B. Staunton, *J. Magn. Magn. Mater.* **448**, 9 (2018).
- [27] P. Strange, A. Svane, W. M. Temmerman, Z. Szotek, and H. Winter, *Nature (London)* **399**, 756 (1999).
- [28] M. Lüders, A. Ernst, M. Däne, Z. Szotek, A. Svane, D. Ködderitzsch, W. Hergert, B. L. Gyorffy, and W. M. Temmerman, *Phys. Rev. B* **71**, 205109 (2005).
- [29] I. D. Hughes, M. Däne, A. Ernst, W. Hergert, M. Lüders, J. P. Poulter, J. B. Staunton, A. Svane, Z. Szotek, and W. M. Temmerman, *Nature (London)* **446**, 650 (2007).
- [30] J. B. Staunton, R. Banerjee, M. dos Santos Dias, A. Deak, and L. Szunyogh, *Phys. Rev. B* **89**, 054427 (2014).
- [31] E. Mendive-Tapia and J. B. Staunton, *Phys. Rev. Lett.* **118**, 197202 (2017).
- [32] H. Ebert, D. Ködderitzsch, and J. Minár, *Rep. Prog. Phys.* **74**, 096501 (2011).
- [33] D. W. Taylor, *Phys. Rev.* **156**, 1017 (1968).
- [34] A. J. Pindor, W. M. Temmerman, and B. L. Gyorffy, *J. Phys. F* **13**, 1627 (1983).
- [35] M. Tsukada, *J. Phys. Soc. Jpn.* **26**, 684 (1969).
- [36] W. H. Butler, *Phys. Rev. B* **8**, 4499 (1973).
- [37] B. L. Gyorffy and G. M. Stocks, in *Electrons in Finite and Infinite Structures*, edited by P. Phariseau and L. Scheire, NATO ASI Series Physics B Vol. 24 (Plenum Press, New York, 1977).
- [38] J. Rossat-Mignod, *J. Physique Colloq.* **40**, C5-95 (1979).
- [39] N. C. Baenziger and J. L. Moriarty, Jr., *Acta Cryst.* **14**, 948 (1961).
- [40] J. A. Blanco, J. I. Espeso, J. G. Soldevilla, J. C. G. Sal, M. R. Ibarra, C. Marquina, and H. E. Fischer, *Phys. Rev. B* **59**, 512 (1999).
- [41] H. Yoshida, S. Abe, T. Kaneko, and K. Kamigaki, *J. Magn. Magn. Mater.* **70**, 275 (1987).
- [42] K. Sekizawa, H. Sekizawa, and C. T. Tomizuka, *J. Phys. Chem. Solids* **31**, 215 (1970).

- [43] U. Köbler, J. Schweizer, P. Chieux, and W. Zinn, *J. Physique, Coll. C8* **49**, 1099 (1988).
- [44] M. M. Amado, R. P. Pinto, M. E. Braga, J. B. Sousa, and P. Morin, *J. Magn. Magn. Mater.* **153**, 107 (1996).
- [45] K. Sekizawa and K. Yasukochi, *Phys. Lett.* **11**, 216 (1964).
- [46] H. B. Lal, *J. Magn. Magn. Mater.* **30**, 192 (1982).
- [47] K. A. Gschneidner, *Acta Cryst.* **18**, 1082 (1965).
- [48] F. Kissel and W. E. Wallace, *J. Less-Common Metals* **11**, 417 (1966).
- [49] G. T. Alfieri, E. Banks, K. Kanematsu, and T. Ohoyama, *J. Phys. Soc. Jpn.* **23**, 507 (1967).
- [50] N. C. Baenziger and J. L. Moriarty, Jr., *Acta Cryst.* **14**, 946 (1961).
- [51] K. Sekizawa, H. Chihara, and K. Yasukochi, *J. Phys. Soc. Jpn.* **50**, 3467 (1981).
- [52] K. Sekizawa, T. Watanabe, and K. Yasukochi, *J. Magn. Magn. Mat.* **31-34**, 181 (1983).
- [53] J. Ruzs, I. Turek, and M. Diviš, *Phys. Rev. B* **71**, 174408 (2005).
- [54] J. Ruzs, I. Turek, and M. Diviš, *J. Alloys Compd.* **408-412**, 930 (2006).
- [55] J. Ruzs, I. Turek, and M. Diviš, *Physica B* **378-380**, 1079 (2006).
- [56] K. H. J. Buschow, G. E. Grechnev, A. Hjelm, Y. Kasamatsu, A. S. Panfilov, and I. V. Svechkarev, *J. Alloys Compd.* **244**, 113 (1996).
- [57] P. Mohn and E. P. Wohlfarth, *J. Phys. F* **17**, 2421 (1987).
- [58] X. B. Liu and Z. Altounian, *Physica B* **406**, 710 (2011).
- [59] L. Vegard, *Z. Physik* **5**, 17 (1921).
- [60] U. Köbler, J. Schweizer, P. Chieux, T. Lorenz, B. Büchner, F. Deloie, and W. Zinn, *J. Magn. Magn. Mater.* **170**, 110 (1997).
- [61] T. Hiraoka, *J. Phys. Soc. Jpn.* **37**, 1238 (1974).
- [62] K. H. J. Buschow, *Rep. Prog. Phys.* **42**, 1373 (1979).
- [63] A. V. Postnikov, V. P. Antropov, and O. Jepsen, *J. Phys.: Condens. Matter* **4**, 2475 (1992).
- [64] J. Schade and M. Neumann, *J. Alloys Compounds* **236**, 132 (1996).
- [65] B. L. Gyorffy and G. M. Stocks, *Phys. Rev. Lett.* **50**, 374 (1983).
- [66] J. B. Staunton, B. L. Gyorffy, G. M. Stocks, and J. Wadsworth, *J. Phys. F: Met. Phys.* **16**, 1761 (1986).